Geophysical Research Letters

RESEARCH LETTER
10.1029/2018GL079390

Key Points:
- Results of aircraft measurements of microphysical properties in a young, soot-rich contrail are presented
- We found a pronounced reduction of ice particle numbers in lower wake regions
- Vertical profiles of soot and ice particle numbers are consistent with soot-controlled ice formation

Supporting Information:
- Supporting Information S1
- Figure S1

Correspondence to:
J. Kleine,
Jonas.Kleine@dlr.de

Citation:
Kleine, J., Voigt, C., Sauer, D., Schlager, H., Scheibe, M., Jurkat-Witschas, T., et al. (2018). In situ observations of ice particle losses in a young persistent contrail. *Geophysical Research Letters*, *45*, 13,553–13,561. https://doi.org/10.1029/2018GL079390

Received 28 JUN 2018
Accepted 20 NOV 2018
Accepted article online 3 DEC 2018
Published online 28 DEC 2018

In Situ Observations of Ice Particle Losses in a Young Persistent Contrail

J. Kleine[1], C. Voigt[1,2], D. Sauer[1], H. Schlager[1], M. Scheibe[1], T. Jurkat-Witschas[1], S. Kaufmann[1], B. Kärcher[1], and B. E. Anderson[3]

[1]Institut für Physik der Atmosphäre, Deutsches Zentrum für Luft- und Raumfahrt (DLR), Wessling, Germany, [2]Institut für Physik der Atmosphäre, Johannes Gutenberg Universität Mainz, Mainz, Germany, [3]NASA Langley Research Center, Hampton, VA, USA

Abstract We describe results of in situ observations of a 1- to 2-min-old contrail in the vortex phase generated from soot-rich exhaust (>10^{15} emitted soot particles per kilogram of fuel burned). Simultaneous measurements of soot (EI_{soot}) and apparent ice (AEI_{ice}) particle number emission indices show a pronounced anticorrelation in the vertical contrail profile. AEI_{ice} decrease by about 75% with increasing distance below the contrail-producing aircraft, while EI_{soot} increase by an equivalent relative fraction, therefore strongly suggesting ice particle formation to be soot-controlled and losses to be caused by sublimation. Quantifying these losses in measurements helps to validate and improve contrail parameterizations used to estimate the climate impact of contrails and contrail cirrus. Our study further demonstrates the challenges in the performance and interpretation of particle measurements in young contrails and lends itself to suggestions for improving contrail data evaluation.

Plain Language Summary Detailed understanding of climatic effects of aircraft contrails and the clouds evolving from them requires accurate in situ measurements. We took measurements in a young persistent contrail that formed at 10 km altitude. We found that a substantial fraction of contrail ice particles is lost shortly after they formed from emissions of copious soot particles from aircraft jet engines. While these results are not entirely unexpected and can be explained by sublimation associated with adiabatic heating in descending aircraft wake vortices, experimental verification is challenging. Importantly, our results increase confidence in the current understanding of processes governing contrail ice formation, growth, and sublimation during early development stages. We provide guidance on quantifying ice particle number concentrations in young contrails and how to relate them to particle emissions. We expect our results to be also beneficial to future studies addressing properties and climate impact of contrails originating from using alternative jet fuels or novel engine technologies.

1. Introduction

Cirrus clouds evolving from aircraft contrails cause the largest contribution to aviation-induced radiative forcing (Burkhardt & Kärcher, 2011; Kärcher, 2018). However, its quantification is affected by significant uncertainties, which underlines the importance to perform appropriate measurements to better understand processes governing contrail formation and evolution (Heymsfield et al., 2010). Though observational data are rare, previous measurements revealed valuable information on microphysical properties of contrails covering consecutive development stages, namely, jet (Baumgardner & Gandrud, 1998; Petzold et al., 1997), vortex (Gayet et al., 2012; Voigt et al., 2010), and dispersion phases (Heymsfield et al., 1998; Schröder et al., 2000; Voigt et al., 2017).

The jet phase corresponds to contrail ages of several seconds and is associated with vigorous plume cooling rates introduced by mixing of the hot exhaust with cold ambient air. Since current soot emission levels are high (>10^{14} particles per kilogram of fuel consumed; Kärcher, 2018), homogeneous freezing of water-activated soot particles is the dominant ice particle formation mechanism (Kärcher & Yu, 2009). In the vortex phase, most of the exhaust and ice particles entrain into two downward-propagating, counter-rotating, wake vortices. Fluid-dynamical models (Huebsch & Lewellen, 2006; Unterstrasser, 2016) and measurements (Jeßberger et al., 2013; Schumann et al., 2013) have shown that aircraft wake dynamics can have marked effects on contrail properties. This includes the possibility of ice particle losses during the descent of wake vortices

forcing ice particle sublimation due to adiabatic heating even if the ambient air surrounding the contrail is ice-supersaturated (Kärcher, 2018; Paoli & Shariff, 2016). Assessing contrail properties toward the end of the vortex phase is of particular interest, as they affect properties of evolving contrail cirrus over hours (Unterstrasser & Gierens, 2010). Establishing a link between contrail ice particles and their precursors in measurements with the help of a model that covers both ice nucleation and sublimation phases was possible only recently (Kärcher & Voigt, 2017) and warrants further scrutiny.

While changes in the initial number of ice particles in contrails have implications for both their lifetime and climate impact (Bier et al., 2017; Schumann et al., 2013), previous analyses of in situ data demonstrated the need to further assess the soot-ice relationship in measurements (Schumann, 2005). Here we analyze in situ data with high temporal resolution in a young contrail in the aircraft wake vortex phase. Besides measuring plume dilution properties and ice particle numbers, the present study provides ancillary measurements of soot particle number concentrations in a contrail that is embedded in an ice-supersaturated environment. As we will show, the data lend themselves to a self-consistent interpretation of the microphysical pathway to contrail ice formation. We offer an in-depth model-data comparison in a separate study (Kärcher et al., 2018). While section 2 outlines the airborne research campaign as well as the instrumentation employed and methods used to analyze the particle data, section 3 presents and discusses the main results.

2. Instrumentation and Methods

Data discussed here were recorded during the flight measurement campaign of the DLR project Emission and Climate Impact of Alternative Fuels (ECLIF), which was conducted over southern Germany in September/October 2015 to investigate the effects of alternative jet fuels and ambient conditions on aircraft emissions and contrail properties. ECLIF employed the DLR Advanced Technology Research Aircraft (ATRA) Airbus A320 equipped with two IAE V2527-A5 engines to burn both standard and specially blended alternative fuels. Exhaust gases, soot particles, and contrail ice particles evolving from the ATRA jet exhaust plumes were probed by instruments installed on the DLR research aircraft Falcon 20-E5. We analyze observations during flight 10 performed on 7 October 2015 during which both ATRA engines burned conventional jet fuel. The ATRA was directed to a flight level of 35,000 ft (≈10.7 km) where a contrail was produced that persisted in ice-supersaturated ambient air. The Falcon probed the entire vertical extent of the young contrail behind the ATRA at ages of 39–132 s.

2.1. General Information

The Falcon meteorological measurement system provided ambient pressure and temperature (238 hPa, 215.5 K at ATRA flight altitude) with accuracies ±0.5 hPa and ±0.5 K (Kaufmann et al., 2014), respectively. Global Positioning System position and altitude with respective uncertainties ±10 and ±15 m were determined by both aircraft individually. Because of systematic discrepancies between Falcon and ATRA in their measurements of pressure altitudes, we evaluated wake vortex descent distances, Δz, based on Global Positioning System altitudes.

We determined water vapor mixing ratios using a CR-2 frost point hygrometer (Buck Research Instruments, LLC; Busen & Buck, 1995; Voigt et al., 2010), connected to a backward-facing inlet to exclude sampling of condensed water. Ambient relative humidities over ice (RHi) measured at the ATRA flight altitude in the air surrounding the contrail ranged from 115% to 125% with an estimated uncertainty of ±15%. The slow response time of the CR-2 in environments characterized by small water vapor mixing ratios prevents us from characterizing RHi within the contrail. With an assumed overall propulsion efficiency of 0.3, the thermodynamic threshold temperature for contrail formation is 224.9 ± 0.7 K (Schumann, 1996). We measured carbon dioxide (CO_2) mixing ratios employing a cavity ring-down analyzer (Picarro CO_2; Rella, 2010). The Picarro sample air was drawn from a backward-facing inlet mounted on the upper Falcon fuselage. Enhancements above background concentrations around 7 ppmv were measured with relative uncertainties of ≤20%. The latter were determined individually for each contrail penetration and are mainly due to precision errors of the instrument and variability in atmospheric background concentrations.

We analyze data in terms of emission indices (EI), defined as mixing ratios relating gas or particle concentrations to the mass of fuel burnt. EI values represent concentrations independent of mixing-induced plume dilution processes. We apply this concept to engine emissions of non-volatile particulate matter (nvPM; essentially aircraft-generated soot particles), as well as to contrail ice particles. In the case of soot, EI gives the number of particles per unit mass of fuel burnt. For contrail ice particle numbers, we use the term apparent

emission index, AEI, since ice particles are not emitted by the jet engines. In this way, soot and ice particle numbers can be directly compared, and any difference between them can be unambiguously associated with microphysical processes. Following Beyersdorf et al. (2014), we calculate particle number emission indices as ratios of enhancements in particle number concentrations above their respective background values (ΔN) to the simultaneously measured CO_2 enhancement (ΔCO_2) by

$$EI_N = \left(\frac{\Delta N}{\Delta CO_2}\right) \cdot \left(\frac{M_{air}}{M_{CO_2}\,\rho_{air}}\right) \cdot EI_{CO_2}\,, \tag{1}$$

with the molar masses of air (M_{air}), CO_2 (M_{CO_2}), and the density of air (ρ_{air}). Linking emissions to the mass of fuel burnt via the passive tracer CO_2 relies on the well-known EI of CO_2 (Schulte & Schlager, 1996); EI_{CO_2} = 3, 158 g/kg for conventional Jet A-1 fuel, assuming 100% combustion efficiency.

2.2. Particle Measurements and Data Analysis

Ice particle size distributions (PSDs) were determined employing the Cloud and Aerosol Spectrometer (CAS) probe (Baumgardner et al., 2001) mounted at a starboard underwing position. The underlying measurement principle is the detection of light scattered by particles within the nominal diameter range 0.5–50 μm in forward direction. Data recorded by a shadow imaging probe that is capable of detecting larger ice particles showed that particles with dimensions >10 μm were present only in comparatively low concentrations (less than about 0.1 cm^{-3}), as expected in fresh contrails (Heymsfield et al., 2010; Voigt et al., 2011), and are therefore not discussed any further.

The CAS was size-calibrated by applying the methods of Rosenberg et al. (2012) and Borrmann et al. (2000), see Supporting Information S1 for details. Ice particle diameters (D_p) are reported here with an uncertainty of ±16%. An analysis of ice particle interarrival times (Field et al., 2003) showed no indication of particle shattering on the CAS probe inlet during contrail penetrations, as expected in the absence of large ice particles. Measured ice particle number concentrations, N_m, are based on a CAS sample area of 0.21 mm^2, as determined by laboratory calibrations, and a calculation of the sample volume following Weigel et al. (2016) using thermodynamic corrections to account for compression effects.

We made an attempt to correct the CAS data for coincidence effects that lead to undercounting biases following Lance (2012). From a detailed instrument intercomparison between the CAS and a modified CAS that was found to be less prone to coincidence artifacts, we derived the empirical coincidence correction function (for details, see Supporting Information S1),

$$N_{CAS} = \alpha(e^{\beta N_m} - 1)\,, \quad \alpha = 1{,}135.43\ cm^{-3}\,, \quad \beta = 1.29 \cdot 10^{-3}\ cm^3\,, \tag{2}$$

with an accuracy of ±12%. By application of equation (2), we derive coincidence corrected number concentrations, N_{CAS}, from concentrations N_m measured by the CAS during ECLIF. We limit the application of this correction to values of $N_m \leq 570\ cm^{-3}$; higher N_m values should not be corrected by this method due to saturation effects of the CAS. However, only N_m values $\leq 522\ cm^{-3}$ (corresponding to $N_{CAS} \leq 1{,}091\ cm^{-3}$) are present in the data set this study is based on. Taking into account additional uncertainties of the sample area determination, flow velocities, and pressures from the CAS sensors, the uncertainty of derived (absolute) contrail ice particle number concentrations is estimated to be ≈25% for N_{CAS} values $\leq 1{,}233\ cm^{-3}$.

High ice particle number concentrations (>10^4 cm^{-3}) nucleate in young, soot-rich contrails (ages <1 s), since otherwise contrails would not be visible at formation (Kärcher et al., 1996). Plume dilution leads to a steady decrease of number concentrations of ice particles right after their formation. Although some cloud probes are less susceptible to coincidence artifacts, we still expect undercounting biases to affect measured data, especially for very high number concentrations exceeding several thousand particles per cubic centimeter. This additional uncertainty is difficult to quantify and hampers the current ability to measure contrail ice particle number concentrations in contrails at ages <10 s. This, however, is less problematic in the present study, since we focus on subsequent vortex regime processes, where excessively high initial ice particle number concentrations have already been significantly reduced by dilution.

Total number concentrations of nvPM particles were determined by a condensation particle counter (CPC, TSI 3010) customized for in-flight use (Fiebig et al., 2005) with a 50% low cutoff diameter of ≃10 nm. Sample air

was drawn from a forward-facing near-isokinetic aerosol inlet mounted on the upper Falcon fuselage about 12 cm laterally apart from the CO_2 inlet. The sample flow was directed through a heated section (≈520 K) removing volatile particle components from the sample. Remaining non-volatile components, assumed to be entirely composed of engine-emitted soot particles, were then detected by the CPC. A switchable dilution section (ratio 1 : 30) enabled the measurement of very high particle number concentrations up to 10^5 cm^{-3} without saturating the counter. Particle counts have been corrected for reduced detection efficiencies in low pressure environments based on laboratory measurements following Noone and Hansson (1990). We determined the overall uncertainty of derived particle number concentrations to be around ±15%.

The interpretation of nvPM measurements in contrails is more challenging than in clear-sky conditions. Since ice particles in soot-rich exhaust form virtually exclusively on emitted soot particles in cold contrails (Kärcher & Yu, 2009), all ice particles contain soot inclusions. With the 50% high cutoff diameter of the aerosol inlet (1.9 μm, for ice particles and conditions of this study calculated following Fiebig, 2001), a significant fraction of contrail ice particles may therefore also be present in the sample flow toward the CPC. After ice particles sublimate completely, soot residues become detectable by the CPC and contribute to EI_{nvPM}, in addition to interstitial soot present in the contrail sample.

This has significant implications for the interpretation of the particle data taken in vortex regime contrails. Ice particles with $D_p = 0.5 - 1.9$ μm are counted by both the CAS and the CPC. This implies that a calculation of total soot particle emissions by adding measured N_{nvPM} and N_{CAS} would suffer from double counting the fraction, f_{05}, of ice particles with $D_p > 0.5$ μm that are transmitted through the aerosol inlet with a size-dependent efficiency, $\mathcal{T}(D_p)$. The latter was derived from laboratory calibrations and is shown in section 3. We correct for this issue by calculating f_{05} by integrating the product of the transfer efficiency of the aerosol inlet and normalized ice PSDs derived from the CAS,

$$f_{05} = \frac{1}{N_{CAS}} \cdot \int_{0.5\,\mu m}^{\infty} \mathcal{T}(D_p) \cdot \frac{dN_{CAS}}{dD_p} \; dD_p. \tag{3}$$

This gives the EI of soot particles with sizes exceeding 10 nm, EI_{soot}, that includes the soot residues contained in ice particles with $D_p < 0.5$ μm:

$$EI_{soot} = EI_{nvPM}(> 10\,nm) - f_{05} \cdot AEI_{ice}, \quad AEI_{ice} = AEI_{CAS}(> 0.5\,\mu m)\,, \tag{4}$$

whereby we derive the AEI of ice particles with $D_p > 0.5$ μm, AEI_{ice}, from the coincidence corrected CAS measurements. We base the following discussion of microphysical processes on EI_{soot} and AEI_{ice} originating from disjoint size spectra of particles.

3. Results and Discussion

Figure 1 shows data from the 25-min measurement sequence of vortex phase contrail properties, on which we base our present study. Contrail data were identified by means of a simultaneous increase in CO_2 mixing ratios (≥1 ppmv) and number concentrations of ice particles with $D_p > 0.5$ μm (≥1 cm^{-3}). Data were sampled in a vertical band of about 135 m height around and below the ATRA flight level. Typically, peak-shaped signal structures with durations 3–20 s resulted from individual contrail penetrations. To calculate EIs, we derived the ratio of particle number to CO_2 concentration enhancements from the ratio of their respective peak areas.

The concomitant detection of high N_{nvPM} values and small N_{CAS} values in contrail samples taken below the ATRA flight altitude (gray-shaded areas in Figure 1) motivates a detailed analysis of the relationship between soot particle emissions and contrail ice particles in terms of the wake vortex descent distance ($\Delta z > 0$). We refer to the upper contrail part as the secondary wake and to the lower part as the primary wake. The latter contains most of the contrail plume and is affected by sinking motion leading to adiabatic heating and sublimation of ice particles even in contrails that form in an ice-supersatured environment (Sussmann & Gierens, 1999; Unterstrasser, 2014).

Vertical profiles of EI_{soot} and AEI_{ice} together with their sum, AEI_{tot}, are shown in Figure 2. We corrected measured nvPM concentrations for double counting (section 2.2); f_{05} values range from 51% in the upper secondary wake to 80% in the lower primary wake. Highest AEI_{ice} values of up to $3.7 \times 10^{15} kg^{-1}$ are found around $\Delta z = -12$ m, with AEI_{ice} showing a decreasing trend with increasing Δz. EI_{soot} exhibits an opposite trend with a maximum value of $4.6 \times 10^{15} kg^{-1}$ at $\Delta z = 105$ m. Artifacts caused by small contrail ice particles impinging

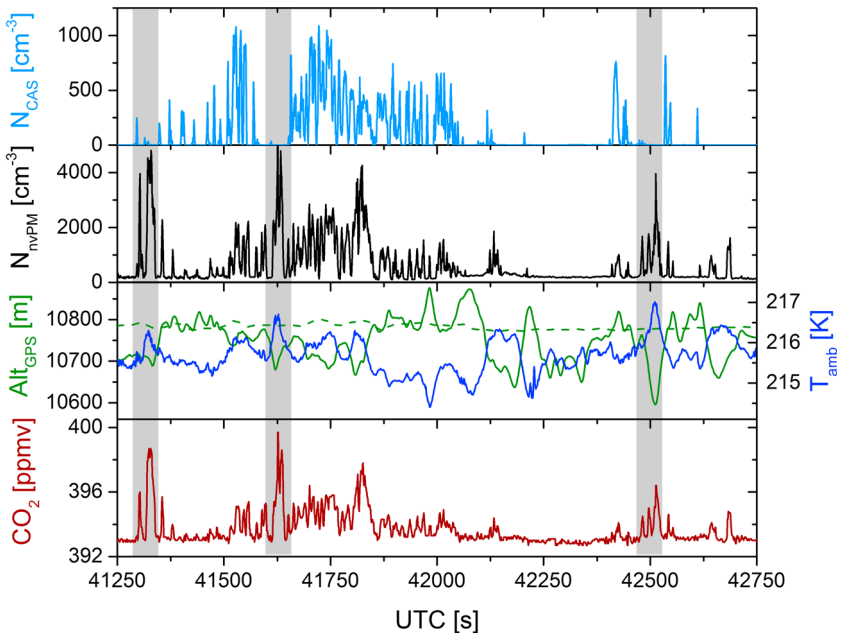

Figure 1. Time series of 1-Hz data observed in the ATRA contrail. Shown are ambient concentrations of ice crystals with $D_p > 0.5$ µm (N_{CAS}) and soot particles from the particle size range 0.01 – 1.9 µm (N_{nvPM}); Falcon GPS altitude and ambient temperature (solid lines); ATRA GPS altitude (dashed line) and CO_2 concentration. Since the Falcon followed the ATRA at slightly lower speed, measurements were taken at contrail ages ranging from 39 to 132 s (wind drift taken into account); the distance between both aircraft increased from 6.9 to 27.1 km. Highest N_{nvPM} are accompanied by low N_{CAS} and local minima in Falcon flight altitude (gray-shaded sequences). The ATRA engine power setting was kept constant during this period (fan speed of 80.5%) which resulted in a measured fuel flow of 1,180 kg/hr per engine on average.
ATRA = Advanced Technology Research Aircraft; CO_2 = carbon dioxide; GPS = Global Positioning System; nvPM = non-volatile matter; CAS = Cloud and Aerosol Spectrometer.

on the aerosol inlet and possibly knocking off deposits of nvPM seem not to be crucial, since highest EI_{soot} values were measured for large Δz, where ice particle concentrations are relatively low.

In the lower wake, a fraction of ice crystals shrinks to sizes below the detection limit of the CAS, including those that sublimate completely thereby releasing their soot cores. This implies a reduction in AEI_{ice} accompanied by an increase in EI_{soot}, explaining the observed anticorrelation between the two variables. Furthermore, there is no significant trend with Δz for AEI_{tot}. This reinforces the notion of soot-controlled ice formation in the analyzed contrail. According to microphysical simulations, volatile plume particles composed of water and sulfate can only contribute to ice formation in low temperature contrails for low soot emissions ($< 10^{14}$ kg^{-1}) (Kärcher & Yu, 2009). A substantial contribution of volatile plume particles to contrail ice formation would not lead to the observed soot-ice anticorrelation.

Taken together, this demonstrates that AEI_{tot} is a suitable measure to quantify total soot particle number emissions in soot-rich contrails during the vortex phase: averaging over the wake depth yields a mean value $AEI_{tot} = 4.9 \times 10^{15}$ kg^{-1} with a sample standard deviation of $\pm 7 \times 10^{14}$ kg^{-1}. Compared to AEI_{ice}, the larger minimum and maximum values found for EI_{soot} may be caused by the contribution of soot residues of ice particles smaller than the detection limit of the CAS to EI_{soot}. Upward mixing of detrained, sublimated ice particles and their respective soot residues might be a second explanation. To a certain degree, this mechanism might also contribute to the observed scatter in derived AEI_{ice} and EI_{soot} data. The presence of interstitial soot in the secondary wake might be a third explanation. However, since 96% of emitted soot particles nucleate ice particles in this contrail (Kärcher et al., 2018), this would imply the sublimation of part of the ice particles near $\Delta z = 0$. This, however, is inconsistent with measured ambient ice supersaturation at the ATRA flight altitude.

We comment on possible sources of scatter in derived AEI_{ice} and EI_{soot} values. First, we recall that CO_2 data are used to convert particle number concentrations to emission indices (section 2.1). We expect that AEI_{ice}

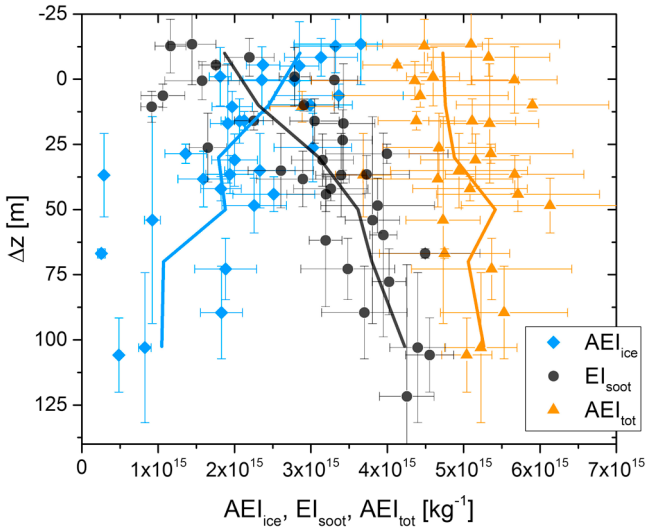

Figure 2. Vertical profiles of AEI_{ice} (blue diamonds), EI_{soot} (black circles), and their sum AEI_{tot} (orange triangles). Δz values > 0 denote altitudes below the flight level of the contrailing ATRA aircraft. The latter is marked by the $\Delta z = 0$ line. To guide the eye, we connect Δz-bin mean values with line segments. Error bars for emission indices represent uncertainties in the determination of CO_2 background levels. Error bars for Δz cover altitude ranges in which data contributing to each plotted point was sampled due to the vertical movement of the Falcon. Corresponding contrail-age-specific vertical profiles are presented in Supporting Information S1. EI = emission index; AEI = apparent emission index.

exhibits a larger scatter than EI_{soot}, because, when compared to the aerosol inlet, the CAS is located at a considerably larger distance (≃4 m perpendicular to flight direction) from the CO_2 inlet. Therefore, spatial inhomogeneities of CO_2 mixing ratios in the plume affect the calculation of AEI_{ice} more than that of EI_{soot}. Second, ground-based measurements during ECLIF suggest up to 20% higher emissions of ATRA engine 2 compared to ATRA engine 1 (Figure S18 in Schripp et al., 2018), causing variability in soot particle numbers already at emission. With the current experimental setup, it is not possible to determine to what degree a given sample of a >1-min-old contrail can be assigned to one specific ATRA engine. Third, radial variability in particle formation conditions in fresh jet plumes causes variability in nucleated ice numbers.

We study the sublimation process further by turning our attention to contrail ice PSDs. Figure 3b shows two contrail ice PSDs from this data set for similar contrail ages, 67 (77) s, taken at different wake levels in the primary (secondary) wake about 100 m apart. The PSDs represent absolute ice particle number concentrations, a normalization relative to CO_2 was not applied.

Total ice particle number concentrations in the primary (secondary) wake are relatively low at this stage of contrail development, 281 (324) cm^{-3}. Effective ice particle diameters, D_{eff} = 1.6 µm (2.3 µm), were determined according to Foot (1988). This means that the associated mean D_p exceed the lower cutoff size of the CAS, so that the measurements capture most (>90%, based on Figure 3b) of the contrail ice particles.

In the lower primary wake, the PSD contains fewer ice particles and shifts toward a smaller mean size relative to the upper secondary wake. Since individual contrail samples were taken at variable positions relative to the contrail core, observed concentration differences might have been caused, in part, by different dilution levels of the individual samples taken. However, together with the decrease in number concentration of large (>1 µm) particles, this more likely suggests that a fraction of ice particles sublimated completely. This notion is supported by the striking agreement of the observed PSDs with model predictions of PSD evolution and shape in descending primary wakes (Figure 3 in Unterstrasser & Sölch, 2010; Figure 7b in Naiman et al., 2011; Figure 18 in Picot et al., 2015; Figure S1 in Kärcher & Voigt, 2017).

We note that the observed PSDs roughly cover size and concentration ranges also found in previous in situ measurements of contrails of comparable age. Baumgardner and Gandrud (1998) and Schröder et al. (2000) report ice particle concentrations of few to several hundred per cubic centimeter with sizes < 10 µm in contrails with ages of ≃30 s and <3 min, respectively. However, a closer intercomparison of contrail ice PSDs from different measurement campaigns and flights is challenging due to variability within one contrail (Figure 3b), as well as dependencies on environmental conditions and source aircraft type (Sussmann & Gierens, 1999; Unterstrasser & Görsch, 2014). Analyses of vertical profiles of microphysical contrail properties (Gayet et al., 2012; Jeßberger et al., 2013) suggest ice PSDs detected in the primary wake being affected by sublimation, in line with the present analysis. While previous measurements (Anderson et al., 1998; Schröder et al., 1998) in the exhaust of various aircraft types detected a wide range of EI_{soot} values, roughly $0.5–10 \times 10^{15}$ kg^{-1}, measurements of AEI_{ice} are sparse. Schumann et al. (2013) derived higher AEI_{ice} in the secondary wake compared to the primary wake; however, they concluded measured ice numbers to be inconsistent with estimates of current soot emission levels, thereby addressing the need for further investigation. While we focus on studying sublimation processes during the vortex phase, we note that ground-based measurements of the ATRA engine 2 exhaust performed during ECLIF report nvPM number EI around $5 - 6 \times 10^{15}$ kg^{-1} (Figure 2b in Schripp et al., 2018) for the same fuel (labeled Ref2 therein) and comparable fuel flow. However, at this point it

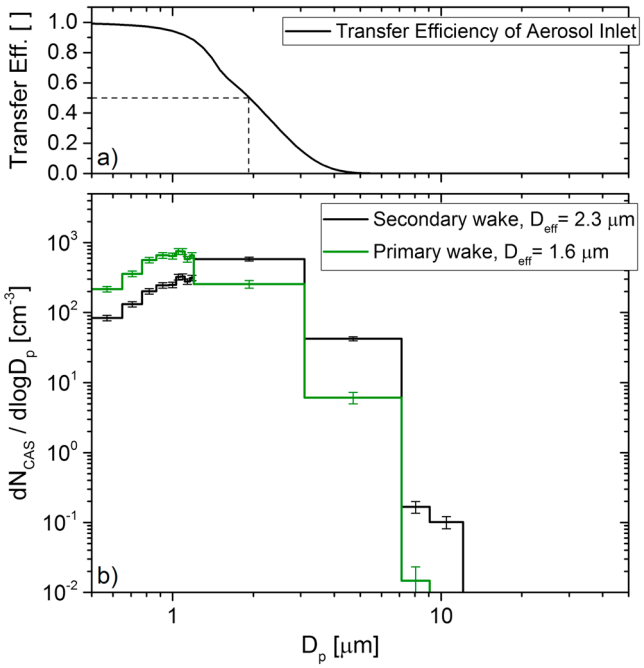

Figure 3. (a) Size-dependent transfer efficiency of ice particles through the aerosol inlet (solid line), $\mathcal{T}(D_p)$, and the related 50% upper cutoff diameter of 1.9 µm (dashed line). (b) Ice particle size distributions detected in the primary (secondary) wake at contrail ages of 67 s (77 s) and corresponding wake depths Δz = 105 m (8 m); averaging periods are 29 s (39) s. Error bars reflect uncertainties of bin mean values due to counting statistics. Similar Δz dependencies of ice particle size distributions were also found for younger (≃40 s) and older (≃130 s) contrail ages (not shown).

remains open to what extent results of ground-based measurements may represent soot emissions at cruise conditions.

4. Summary and Outlook

This study reports on in situ measurements of soot and ice particle properties in a persistent contrail during the wake vortex regime. We described the methods employed to analyze the data and studied the interdependence of soot and ice particle numbers as a function of aircraft wake position below the contrailing aircraft.

Without accounting for the overlap in contrail measurements of soot particles included in ice crystals from the CAS and CPC instruments, we would not be able to offer a self-consistent interpretation of the data regarding ice formation and sublimation processes. While this interpretation is in line with mechanisms currently implemented in models, most of those models have not been validated regarding the magnitude of predicted sublimation losses, as measured data were evaluated with different focus (e.g., Febvre et al., 2009; Kaufmann et al., 2014; Voigt et al., 2011). Validation, however, is required owing to the uncertainty in microphysical parameters determining sublimation rates (Kärcher & Voigt, 2017).

By juxtaposing vertical profiles of soot and ice particle numbers in the contrail during the vortex descent, our results strongly suggest sublimation to substantially effect ice numbers in soot-rich contrails. Furthermore, they provide strong evidence that the contrail ice particles indeed nucleated on the emitted soot particles. We further analyze sublimation mechanisms and quantify the associated ice particle losses to predictions by means of a parameterization scheme for contrail ice formation that covers both, nucleation and sublimation phases, in the companion paper (Kärcher et al., 2018).

We conclude our study by pointing to a number of issues for further investigation. First, future contrail studies would greatly benefit from better experimental constraints on the size distributions in the size range 1–100 nm and total number of soot particles emitted from jet engines. These size spectra could be measured in contrail situations and ideally take into account engine-to-engine variability in flight. Second, direct measurements of nucleated ice particle concentrations in fresh contrails require instrumental approaches that are unaffected by coincidence issues and at the same time probe the relevant particle size range 0.1–10 µm. Third, more experimental data on total ice crystal numbers, their size distribution, and vertical profiles across the wake at the end of the contrail formation stage (age 5–10 min) are needed to initialize contrail properties in models simulating atmospheric effects of persistent contrails and contrail cirrus. Fourth, ice crystal sublimation processes have to be considered in studies assessing the effects novel engine technologies (Boies et al., 2015) or alternative fuels (Moore et al., 2017) exert on contrail properties and their climate impact. Fifth, a closer comparison of ground-based and in-flight soot measurements requires comparable engine operation conditions and instrumentation.

Acknowledgments
This study was carried out within the DLR project ECLIF (Emission and Climate Impact of Alternative Fuels). C. V. acknowledges funding by the Helmholtz Society under contract W2/W3-60. We are grateful to Beiping Luo for providing us with T-matrix calculations for nonabsorbing ice crystals. Data used in this study are archived at HALO database (https://halo-db.pa.op.dlr.de).

References

Anderson, B. E., Cofer, W. R., Bagwell, D. R., Barrick, J. W., Hudgins, C. H., & Brunke, K. E. (1998). Airborne observations of aircraft aerosol emissions I: Total nonvolatile particle emission indices. *Geophysical Research Letters*, *25*(10), 1689–1692.

Baumgardner, D., & Gandrud, B. E. (1998). A comparison of the microphysical and optical properties of particles in an aircraft contrail and mountain wave cloud. *Geophysical Research Letters*, *25*(8), 1129–1132.

Baumgardner, D., Jonsson, H., Dawson, W., O'Connor, D., & Newton, R. (2001). The cloud, aerosol and precipitation spectrometer: A new instrument for cloud investigations. *Atmospheric Research*, *59*, 251–264.

Beyersdorf, A. J., Timko, M. T., Ziemba, L. D., Bulzan, D., Corporan, E., Herndon, S. C., et al. (2014). Reductions in aircraft particulate emissions due to the use of Fischer–Tropsch fuels. *Atmospheric Chemistry and Physics*, *14*(1), 11–23.

Bier, A., Burkhardt, U., & Bock, L. (2017). Synoptic control of contrail cirrus life cycles and their modification due to reduced soot number emissions. *Journal Geophysical Research: Atmospheres*, *122*, 11,584–11,603. https://doi.org/10.1002/2017JD027011

Boies, A. M., Stettler, M. E., Swanson, J. J., Johnson, T. J., Olfert, J. S., Johnson, M., et al. (2015). Particle emission characteristics of a gas turbine with a double annular combustor. *Aerosol Science and Technology*, *49*(9), 842–855.

Borrmann, S., Luo, B., & Mishchenko, M. (2000). Application of the T-matrix method to the measurement of aspherical (ellipsoidal) particles with forward scattering optical particle counters. *Journal of Aerosol Science*, *31*(7), 789–799.
Burkhardt, U., & Kärcher, B. (2011). Global radiative forcing from contrail cirrus. *Nature Climate Change*, *1*(1), 54–58.
Busen, R., & Buck, A. L. (1995). A high-performance hygrometer for aircraft use: Description, installation, and flight data. *Journal of Atmospheric and Oceanic Technology*, *12*(1), 73–84.
Febvre, G., Gayet, J. F., Minikin, A., Schlager, H., Shcherbakov, V., Jourdan, O., et al. (2009). On optical and microphysical characteristics of contrails and cirrus. *Journal of Geophysical Research*, *114*, D02204. https://doi.org/10.1029/2008JD010184
Fiebig, M. (2001). Das troposphärische Aerosol in mittleren Breiten Mikrophysik, Optik und Klimaantrieb am Beispiel der Feldstudie LACE 98 (PhD thesis), Ludwig-Maximilians-Universität, München.
Fiebig, M., Stein, C., Schröder, F., Feldpausch, P., & Petzold, A. (2005). Inversion of data containing information on the aerosol particle size distribution using multiple instruments. *Journal of Aerosol Science*, *36*(11), 1353–1372. https://doi.org/10.1016/j.jaerosci.2005.01.004
Field, P. R., Wood, R., Brown, P. R. A., Kaye, P. H., Hirst, E., Greenaway, R., & Smith, J. A. (2003). Ice particle interarrival times measured with a fast FSSP. *Journal of Atmospheric and Oceanic Technology*, *20*(2), 249–261.
Foot, J. S. (1988). Some observations of the optical properties of clouds. II: Cirrus. *Quarterly Journal of the Royal Meteorological Society*, *114*(479), 145–164.
Gayet, J.-F., Shcherbakov, V., Voigt, C., Schumann, U., Schäuble, D., Jessberger, P., et al. (2012). The evolution of microphysical and optical properties of an A380 contrail in the vortex phase. *Atmospheric Chemistry and Physics*, *12*(14), 6629–6643. https://doi.org/10.5194/acp-12-6629-2012
Heymsfield, A., Baumgardner, D., DeMott, P., Forster, P., Gierens, K., & Kärcher, B. (2010). Contrail microphysics. *Bulletin of the American Meteorological Society*, *91*(4), 465–472.
Heymsfield, A. J., Lawson, R. P., & Sachse, G. W. (1998). Growth of ice crystals in a precipitating contrail. *Geophysical Research Letters*, *25*(9), 1335–1338.
Huebsch, W., & Lewellen, D. (2006). Sensitivity study on contrail evolution. In *36th AIAA Fluid Dynamics Conference and Exhibit, AIAA 2006–3749* (pp. 1–14).
Jeßberger, P., Voigt, C., Schumann, U., Sölch, I., Schlager, H., Kaufmann, S., et al. (2013). Aircraft type influence on contrail properties. *Atmospheric Chemistry and Physics*, *13*(23), 11,965–11,984. https://doi.org/10.5194/acp-13-11965-2013
Kärcher, B. (2018). Formation and radiative forcing of contrail cirrus. *Nature Communications*, *9*(1), 1824. https://doi.org/10.1038/s41467-018-04068-0
Kärcher, B., Kleine, J., Sauer, D., & Voigt, C. (2018). Contrail formation: Analysis of sublimation mechanisms. *Geophysical Research Letters*, *45*. https://doi.org/10.1029/2018GL079391
Kärcher, B., Peter, T., Biermann, U. M., & Schumann, U. (1996). The initial composition of jet condensation trails. *Journal of the Atmospheric Sciences*, *53*(21), 3066–3083.
Kärcher, B., & Voigt, C. (2017). Susceptibility of contrail ice crystal numbers to aircraft soot particle emissions. *Geophysical Research Letters*, *44*, 8037–8046. https://doi.org/10.1002/2017GL074949
Kärcher, B., & Yu, F. (2009). Role of aircraft soot emissions in contrail formation. *Geophysical Research Letters*, *36*, L01804. https://doi.org/10.1029/2008GL036649
Kaufmann, S., Voigt, C., Jeberger, P., Jurkat, T., Schlager, H., Schwarzenboeck, A., et al. (2014). In situ measurements of ice saturation in young contrails. *Geophysical Research Letters*, *41*, 702–709. https://doi.org/10.1002/2013GL058276
Lance, S. (2012). Coincidence errors in a Cloud Croplet Probe (CDP) and a Cloud and Aerosol Spectrometer (CAS), and the improved performance of a modified CDP. *Journal of Atmospheric and Oceanic Technology*, *29*(10), 1532–1541.
Moore, R. H., Thornhill, K. L., Weinzierl, B., Sauer, D., D'Ascoli, E., Kim, J., et al. (2017). Biofuel blending reduces particle emissions from aircraft engines at cruise conditions. *Nature*, *543*, 411–415.
Naiman, A. D., Lele, S. K., & Jacobson, M. Z. (2011). Large eddy simulations of contrail development: Sensitivity to initial and ambient conditions over first twenty minutes. *Journal of Geophysical Research*, *116*, D21208. https://doi.org/10.1029/2011JD015806
Noone, K. J., & Hansson, H. C. (1990). Calibration of the TSI 3760 condensation nucleus counter for nonstandard operating conditions. *Aerosol Science and Technology*, *13*(4), 478–485. https://doi.org/10.1080/02786829008959462
Paoli, R., & Shariff, K. (2016). Contrail modeling and simulation. *Annual Review of Fluid Mechanics*, *48*, 393–427.
Petzold, A., Busen, R., Schröder, F. P., Baumann, R., Kuhn, M., Ström, J., et al. (1997). Nearfield measurements on contrail properties from fuels with different sulfur content. *Journal of Geophysical Research*, *102*(D25), 29,867–29,880.
Picot, J., Paoli, R., Thouron, O., & Cariolle, D. (2015). Large-eddy simulation of contrail evolution in the vortex phase and its interaction with atmospheric turbulence. *Atmospheric Chemistry and Physics*, *15*, 7369–7389.
Rella, C. (2010). Accurate greenhouse gas measurements in humid gas streams using the Picarro G1301 carbon dioxide / methane / water vapor gas analyzer. White Paper from Picarro Inc., Sunnyvale, CA.
Rosenberg, P. D., Dean, A. R., Williams, P. I., Dorsey, J. R., Minikin, A., Pickering, M. A., & Petzold, A. (2012). Particle sizing calibration with refractive index correction for light scattering optical particle counters and impacts upon PCASP and CDP data collected during the Fennec campaign. *Atmospheric Measurement Techniques*, *5*(5), 1147–1163.
Schripp, T., Anderson, B. E., Crosbie, E., Moore, R. H., Herrmann, F., Osswald, P., et al. (2018). Impact of alternative jet fuels on engine exhaust composition during the 2015 ECLIF Ground-Based Measurements Campaign. *Environmental Science & Technology*, *52*(8), 4969–4978. https://doi.org/10.1021/acs.est.7b06244
Schröder, F., Kärcher, B., Duroure, C., Strm, J., Petzold, A., Gayet, J. F., et al. (2000). On the transition of contrails into cirrus clouds. *Journal of the Atmospheric Sciences*, *57*(4), 464–480.
Schröder, F. P., Kärcher, B., Petzold, A., Baumann, R., Busen, R., Hoell, C., & Schumann, U. (1998). Ultrafine aerosol particles in aircraft plumes: In situ observations. *Geophysical Research Letters*, *25*(15), 2789–2792.
Schulte, P., & Schlager, H. (1996). In-flight measurements of cruise altitude nitric oxide emission indices of commercial jet aircraft. *Geophysical Research Letters*, *23*(2), 165–168. https://doi.org/10.1029/95GL03691
Schumann, U. (1996). On conditions for contrail formation from aircraft exhausts. *Meteorologische Zeitschrift*, *5*, 4–23.
Schumann, U. (2005). Formation, properties and climate effects of contrails. *Calum Raistrick Physique*, *6*, 549–565.
Schumann, U., Jeßberger, P., & Voigt, C. (2013). Contrail ice particles in aircraft wakes and their climatic importance. *Geophysical Research Letters*, *40*, 2867–2872. https://doi.org/10.1002/grl.50539
Sussmann, R., & Gierens, K. M. (1999). Lidar and numerical studies on the different evolution of vortex pair and secondary wake in young contrails. *Journal of Geophysical Research*, *104*(D2), 2131–2142.
Unterstrasser, S. (2014). Large-eddy simulation study of contrail microphysics and geometry during the vortex phase and consequences on contrail-to-cirrus transition. *Journal of Geophysical Research: Atmospheres*, *119*, 7537–7555. https://doi.org/10.1002/2013JD021418

Unterstrasser, S. (2016). Properties of young contrails-a parametrisation based on large-eddy simulations. *Atmospheric Chemistry and Physics*, *16*(4), 2059–2082.

Unterstrasser, S., & Gierens, K. (2010). Numerical simulations of contrail-to-cirrus transition—Part 2: Impact of initial ice crystal number, radiation, stratification, secondary nucleation and layer depth. *Atmospheric Chemistry and Physics*, *10*(4), 2037–2051. https://doi.org/10.5194/acp-10-2037-2010

Unterstrasser, S., & Görsch, N. (2014). Aircraft-type dependency of contrail evolution. *Journal of Geophysical Research: Atmospheres*, *119*, 14,015–14,027. https://doi.org/10.1002/2014JD022642

Unterstrasser, S., & Sölch, I. (2010). Study of contrail microphysics in the vortex phase with a Lagrangian particle tracking model. *Atmospheric Chemistry and Physics*, *10*(20), 10,003–10,015.

Voigt, C., Schumann, U., Jessberger, P., Jurkat, T., Petzold, A., Gayet, J. F., et al. (2011). Extinction and optical depth of contrails. *Geophysical Research Letters*, *38*, L11806. https://doi.org/10.1029/2011GL047189

Voigt, C., Schumann, U., Minikin, A., Abdelmonem, A., Afchine, A., Borrmann, S., et al. (2017). ML-CIRRUS: The airborne experiment on natural cirrus and contrail cirrus with the high-altitude long-range research aircraft HALO. *Bulletin of the American Meteorological Society*, *98*(2), 271–288. https://doi.org/10.1175/BAMS-D-15-00213.1

Voigt, C., Schumann, U., Schmale, J., Jessberger, P., Hamburger, T., Lichtenstern, M., et al. (2010). In-situ observations of young contrails-overview and selected results from the CONCERT campaign. *Atmospheric Chemistry and Physics*, *10*(18), 9039–9056.

Weigel, R., Spichtinger, P., Mahnke, C., Klingebiel, M., Afchine, A., Petzold, A., et al. (2016). Thermodynamic correction of particle concentrations measured by underwing probes on fast-flying aircraft. *Atmospheric Measurement Techniques*, *9*(10), 5135.